Journal of Mechatronics, Electrical Power, and Vehicular Technology 16 (2025) 106-118

Journal of Mechatronics, Electrical Power, and Vehicular Technology

e-ISSN: 2088-6985
p-ISSN: 2087-3379

mev.brin.go.id

Artificial intelligence for field-oriented control on light rail transit Jabodebek

Wahyu Pribadi [a], Ricto Yudi Wicaksono [a, *], Rakhmad Gusta Putra [a], Darma Arif Wicaksono [a], Moh. Lutfi Yazid [b]

[a] *Rolling Stock Engineering Departement of Politeknik Negeri Madiun*
West Ringroad Street Winongo Madiun, Madiun, 63162, Indonesia

[b] *Quality Control Department of PT INKA*
71 Yos Sudarso Street, Madiun, 63162, Indonesia

Abstract

The increasing number of vehicles in Jakarta, Indonesia, has had a negative impact on the environment. If this trend continues, it may significantly harm public health. In response to this issue, the government has introduced mass transportation solutions, such as the Jabodebek light rail transit (LRT) system. One of the key technical challenges in operating the LRT is ensuring smooth and reliable traction motor control. This study presents a simulation of the Jabodebek LRT's traction motor performance when traversing a hilly route with a 29 ‰ gradient. A field-oriented control (FOC) method is implemented to regulate motor speed. The train operates under a constant load, with its weight gradually increasing from the lowest to the highest point of the slope. Two tuning methods are applied to optimize the controller parameters: manual (hand-tuning) and artificial intelligence-based optimization using the Firefly algorithm and the Grey Wolf optimizer (GWO). The integral of time multiplied by absolute error (ITAE) is used as the objective function to evaluate the speed control performance. The simulation results show that the Grey Wolf optimizer delivers the best performance, achieving stable speed control despite load disturbances. The optimal proportional and integral gains obtained are Kp = 16.233861 and Ki = 0.526774, respectively.

Keywords: field-oriented control; firefly algorithm; Grey Wolf algorithm; integral of time multiplied by absolute error (ITAE); LRT Jabodebek.

I. Introduction

Traffic congestion is a significant issue for the residents of DKI Jakarta. The high density of vehicles contributes to increased emissions, particularly from motor vehicles. In 2022, the average concentration of carbon monoxide (CO) in Jakarta was recorded at 897 μg/m³, based on measurements taken from five monitoring locations [1]. This situation poses a serious threat to the health of DKI Jakarta residents. In response, the government has initiated the development of additional infrastructure, such as the Jabodebek light rail transit (LRT), to help reduce the number of motorized vehicles and alleviate traffic congestion [2].

Various studies on electric trains are being actively conducted to achieve optimal energy efficiency with minimal environmental impact. One such approach involves the integration of traction batteries, which can

* Corresponding Author. ricto@pnm.ac.id (R. Y. Wicaksono)

https://doi.org/10.55981/j.mev.2025.1061

Received 19 February 2025; 1st revision 19 June 2025; 2nd revision 26 June 2025; accepted 30 June 2025; available online 31 July 2025; published 31 July 2025

How to Cite: W. Pribadi, *et al.*, "Artificial intelligence for field-oriented control on light rail transit Jabodebek," *Journal of Mechatronics, Electrical Power, and Vehicular Technology*, vol. 16, no. 1, pp. 106-118, July, 2025.

enhance the affordability and sustainability of the electrical energy consumed by electric trains [3]. In addition, issues related to the drive system must also be taken into account, as operating an electric train typically requires more than one traction motor. Therefore, the drive system should be capable of optimally supplying electrical power to each traction motor to ensure efficient operation [4].

Direct current (DC) motors are relatively easy to control and cost-effective [5]. However, induction motors offer advantages in terms of weight and size, as they are lighter and more compact while delivering the same power output, making them highly suitable for traction motor applications. In terms of load-handling capability, induction motors are well-equipped to deliver high torque [6], output power [7], and they perform reliably under varying load conditions [8].

The drive's ability to move the motor on an electric train is very necessary to maintain the stability of the motor in motion, especially when passing over loads, namely, uphill tracks. Based on [9], the maximum gradient that can be passed by trains in class 1 and 2 is 10 ‰, 20 ‰ in class 3. In class 4 and 5, it is 25 ‰. However, on the Jabodebek LRT route, the maximum gradient is 29 ‰, which can still increase the torque pull from the train traction motor [10].

Several control methods have been developed to optimize the performance of induction motors. Direct torque control (DTC) offers a fast torque response with high efficiency and is advantageous due to its simple construction, ease of maintenance, and low cost [6]. However, this method also presents several notable drawbacks. First, it involves increased computational complexity, which may demand more advanced processing capabilities and extended calculation time [11]. Second, it tends to generate higher torque ripple, which can adversely affect the smoothness and efficiency of motor operation [12]. Additionally, the method is often sensitive to parameter variations [13] and may encounter challenges related to switching frequency and electromagnetic noise [14].

Sliding mode control (SMC) enables the motor to accurately track the desired speed or position, particularly under ideal operating conditions. Nonetheless, one of its primary limitations is the inherent chattering phenomenon, which results from the discontinuous control law and switching action used to maintain the sliding condition [15]. Another widely used method is field-oriented control (FOC), also known as vector control, which provides effective control across a broad torque and speed range. It is generally easier to implement, more robust to parameter variations, and offers smoother operation with lower torque ripple and noise [16][17].

Regarding the calculations, PI tuning can be done using the Ziegler-Nichols method as in [18]. The results of this study with proportional gain (Kp), integral gain (Ki), derivative gain (Kd) of 0.4, 0.008, and 9 can maintain speed at a load of 4 kg, and tasekkes 5.8 seconds to return to the setpoint. Towards the modern era, control of a system must be able to adjust automatically, which is combined with artificial intelligence (AI) [19].

When the FOC is implemented with different AI, it will produce different results. The first method, neural network, can be applied to all applications, but the processing time is large. The second method is a fuzzy logic controller, which can achieve stability in a short time, but this method has a small control interval or is limited by the rule. The third is genetic algorithm (GA). This method can be applied to high noise [20].

Modern study has explored advanced AI methods for PI controller tuning, including the Firefly algorithm (FYA). In [21], FYA was applied to optimize the Kp, Ki, and Kd parameters of a DC-DC boost converter, resulting in improvements in rise time, settling time, overshoot, and peak response. Another new AI is the Grey Wolf algorithm (GWO). Research in [22] implemented GWO for tuning a sliding mode controller in a dual star induction motor, demonstrating better performance compared to indirect field-oriented control (FOC). GWO successfully tunes the PID parameters to improve system performance, where traditional analytical methods fail due to the high-order complexity of the micro hydro power plant. In off-grid and on-grid systems, GWO-tuned controllers achieve a faster settling time and reach steady-state conditions more quickly [23].

Based on this background, this study proposes the design of an FOC-based control system for a three-phase induction motor used in the Jabodebek LRT traction system. The FYA and GWO algorithms are employed to determine the optimal Kp and Ki values based on the integral of time multiplied by absolute error (ITAE) objective function.

II. Materials and Methods

A. Field oriented control

This is one of the modern and advanced method control for induction motor. This technique provides precise control of an induction motor's speed and torque by controlling the motor's magnetic field. It offers improved performance, efficiency, and reliability compared to traditional VFD control methods [24][25].

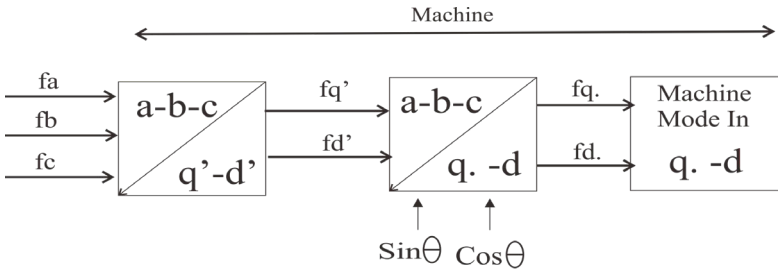

Figure 1. Side machine transformation in FOC.

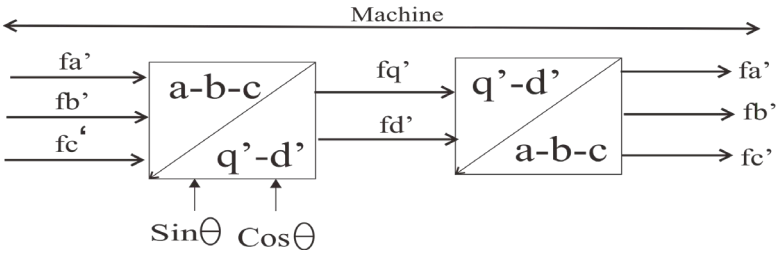

Figure 2. Variable transformation in FOC.

The FOC method can be carried out by involving several steps.

First, the FOC technique is carried out by transforming the variables of the three-phase system *a-b-c* to the two-phase stationary frame (*q-d*) and re-transforming them into the angular velocity ω, which can be seen in Figure 1 of the FOC machine transformation and the FOC transformation variables in Figure 2. At this stage, the three-phase current values a, b, c are obtained from a, b, which can be expressed as equation (1) and equation (2).

$$fa + fb + fc = 0 \quad (1)$$

so

$$fc = -(fa + fb) \quad (2)$$

Secondly, the FOC technique must apply the Clarke transformation to change *iabc* to *fαβ*. The new current variable is a quadrature current that changes with time. This can be stated as equation (3).

$$fa + fb + fc = 0 \quad (3)$$

which can also be stated as equation (4) and equation (5).

$$fa = \frac{2}{3} fa + \frac{1}{3} fb + \frac{1}{3} fc = 0 \quad (4)$$

$$f\beta = \frac{1}{\sqrt{3}} (fb - fc) \quad (5)$$

substitution of equation (3), equation (4), equation (5) to produce equation (6) and equation (7).

$$fa = fa \quad (6)$$

$$f\beta = \frac{1}{\sqrt{3}} (fa + 2fb) \quad (7)$$

Then apply the Park transform to convert *fαβ* to fdq, utilizing the given transform angle (which is the rotor flux linkage position). The stator current should be used to calculate the rotor flux and transform angle using the induction motor slip equation. The inverse Clarke is then used to find *fdq*, which can be expressed as equation (8) and equation (9).

$fa = fa$

$$fb = \frac{-fa + \sqrt{3} \times f\beta}{2} \quad (8)$$

$$fb = \frac{-fa - \sqrt{3} \times f\beta}{2} \quad (9)$$

In the FOC technique, park transformation is needed to take three-phase stator current (*ia*, *ib*, *ic*) and convert it into two orthogonal components (*id*, *iq*) in the *dq* framework. This transformation is done by the *id* component representing the direct axis (flux producing component) and the *iq* component representing the quadrature axis (torque producing component).

This transformation is divided into two, namely forward and reverse. The forward Park transformation, also known as the Clarke-Park transformation, converts three-phase quantities (eg, stator currents *fa*, *fb*, *fc*) into a two-phase orthogonal coordinate system (*dq* frame). This transformation is used to simplify the control structure and separate the flux and torque components, which can be expressed as equation (10) and equation (11).

$$fa = fd \cos\theta - fq \sin\theta \quad (10)$$

$$fb = fd \sin\theta + fq \cos\theta \quad (11)$$

The inverse Park transform also known as the inverse Clarke-Park transform, converts the two-phase dq order components back into the three-phase quantities *fa*, *fb*, and *fc*. Which can be expressed as equation (12) and equation (13).

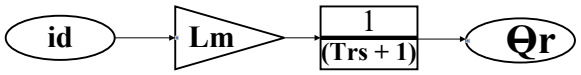

Figure 3. Flux calculation block diagram.

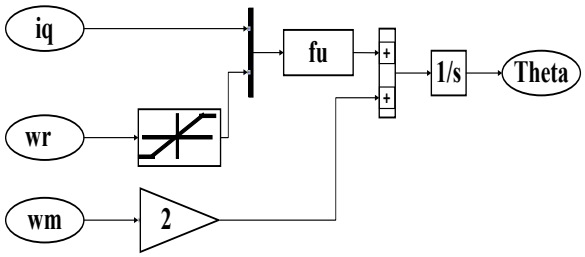

Figure 4. Theta calculation block diagram.

$$fd = f\alpha \cos\theta + f\beta \sin\theta \quad (12)$$

$$fq = -f\alpha \sin\theta + f\beta \cos\theta \quad (13)$$

B. Squirrel-cage induction motor

Such as all induction machines, this machine is an asynchronous machine with a speed that depends on the applied frequency, number of poles, and load torque [24]. The operating speed of the motor is determined by equation (14).

$$ns = \frac{120 \times f}{p}(1\text{-}s) \quad (14)$$

The *ns* value is the motor speed in rpm unit. The frequency is expressed by f with Hz unit and p is pole. After knowing the speed value, the synchronous angular velocity can also be known which is expressed in equation (15).

$$\omega s = \frac{2\pi ns}{60} \quad (15)$$

Synchronous angular velocity is expressed in rad/s. Nominal slip can be expressed in equation (16).

$$S = \frac{\omega s - \omega m}{\omega s} \times 100\% \quad (16)$$

The calculation of the rotor flux of the induction motor represented in Figure 3 can be estimated using the stator current and rotor parameters as equation (17).

$$\varphi r = \frac{Lm \times fqs}{Trs + 1} \quad (17)$$

Theta calculation is explained in Figure 4. Adding the electric velocity and the slip velocity through an integrator will give the theta for the transformation, which can be expressed as equation (18). The d-axis equivalent and q-axis equivalent circuit induction motor are illustrated in Figure 5 which help to calculate slip velocity in equation (18) and torque *Te* in equation (19).

$$\omega s = \frac{Lm \times fqs}{Tr \times \varphi r} + \frac{p}{2} \times \omega m \quad (18)$$

Thus, according to equation (18), it can calculate the value of torque *Te* from *fqs* as equation (19).

$$Te = \frac{3 \times p \times Lm \times \varphi r \times fqs}{4 \times Lr} \quad (19)$$

Based on equation (19), the *fq* reference value *fq_ref* can be determined as equation (20).

$$fq\_ref = \left(\frac{4 \times Lr \times Te}{3 \times p \times Lm}\right) / \varphi r \quad (20)$$

Induction motors also have a friction coefficient B, constant inertia *J*, reference speed ωm^* and actual or rotor speed *ωs*, which mathematically can be expressed in equation (21).

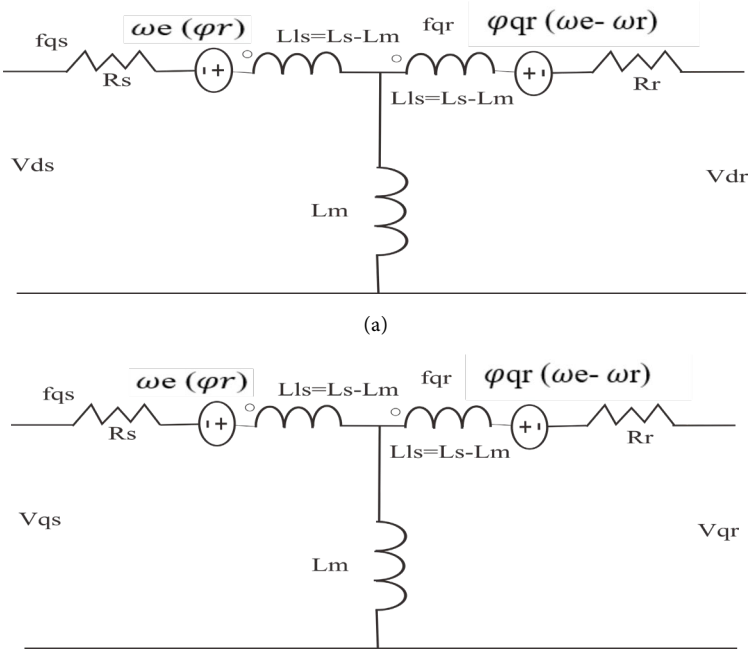

Figure 5. (a) d-axis equivalent and (b) q-axis equivalent circuit induction motor.

$$\frac{\omega m}{Te} = \frac{1}{Js+B} \quad (21)$$

In this induction motor modeling, the LRT Jabodebek traction motor is used. This traction motor is selected as 1 traction motor from the main cabin. Table 1 is the specification of the three-phase induction traction motor [10].

C. Design AI-control

In the FOC method, there is a PI gain that can determine the stability of the motor speed. The PI calculation method is carried out in 3 ways, namely hand-tuning, Firefly algorithm (FYA), and Grey Wolf algorithm (GWO). Each PI tuning algorithm requires an objective function.

The integral of time multiplied by absolute error (ITAE) is used as the objective function in [26]. This is because this method can provide the difference between motor speed and actual speed. The two parameters will be evaluated and can be given the optimal Kp and Ki values. ITAE can be expressed in equation (22).

$$\text{ITAE} = \int_0^{\sim} t|e(t)|dt \quad (22)$$

1) Firefly algorithm (FYA)

FYA is an algorithm that imitates the habits of fireflies [27]. Each firefly will follow the firefly with better light intensity. For the brightest firefly, it will perform a local search by moving randomly in its environment. If firefly *j* is brighter than firefly *i*, then firefly *i* will move towards firefly *j* using the update formula given in equation (23).

$$xt = xi + \beta_0 e^{-\gamma r_0^2} (x_j - xi) + \alpha(\varepsilon() - 0.5) \quad (23)$$

where β_0 is the attractiveness of *xj* at $r = 0$. γ is an algorithm parameter that determines the degree to which the updating process depends on the distance between the two fireflies. Moreover, α is an algorithm parameter for the step length of the random movement and $\varepsilon()$ is a random vector from a uniform distribution with values between 0 and 1. For the brightest firefly, *xb*, the second expression is explained in equation (24).

$$x_b = x_b + \alpha\,\alpha(\varepsilon()\text{-}0.5 \quad (24)$$

Several parameters and FYA values used to calculate PI for FOC in this study are shown in Table 2.

2) Grey Wolf algorithm (GWO)

This is a new evolutionary algorithm-based optimization technique inspired by gray wolves. This behaviour is based on the behaviour of the Grey Wolf in question tracking, chasing, and approaching the prey, encircling and harassing the prey until it stops moving, and ultimately attacking the prey [22][28].

There are several subjects in this AI, such as Alpha (α), Beta (β), Delta (δ), and Omega (ω) that represent the Grey Wolf level and solutions [29]. The initial size and number can be calculated in equation (25).

$$W = lowerbound + rand \times (Ub\text{-}Lb) \quad (25)$$

W show the initial value of wolves while rand is random. *Ub* and *Lb* is the bound value for upper and lower that are used in this calculation. Next, the method calculates the first best position ($X\alpha$), second best position ($X\beta$), and third best position ($X\delta$). The calculation in three positions or solutions are expressed in equation (26), equation (27), equation (28), equation (29), equation (30).

$$X1 = X\alpha - A1 \times D \quad (26)$$

$$A1 = 2 \times \alpha \times rand - \alpha \quad (27)$$

$$A = 2 \times (1\text{-}iteration/max\ iteration) \quad (28)$$

$$C1 = 2 \times rand \quad (29)$$

$$D = |C1 \times X\alpha - X(t)| \quad (30)$$

where *x(t)* is the current iteration, *A1* and *C1* are the coefficient vector. This method is also used in *X2* and *X3*. The new position of wolves can be expressed as equation (31).

Table 1.
Specification of the induction motor of LRT Jabodebek.

Parameter and symbol	Value and unit
Stator resistance (Rs)	0.35 Ω
Rotor resistance (R2)	0.07 Ω
Stator inductivity (L1)	0.0025 H
Rotor inductivity (L2)	0.00125 H
Mutual inductivity (Lm)	0.0028 H
Frequency(fz)	60 Hz
Pole (p)	4
Nominal speed (N)	1554 rpm
Nominal power	90000 Watt
Inertia (J)	0.43

Table 2.
The specification of FYA.

Parameter and symbol	Value
Number Firefly	20
Alpha (α)	0.1
Beta (β)	0.9
Upper bound (Ub)	Kp = 30, Ki = 10
Lower bound (Lb)	Kp = 10, Ki = 0
Objective function	ITAE

Table 3.
The specification of GWO.

Parameter and symbol	Value
Number Firefly	20
Alpha (α)	0.1
Beta (β)	0.9
Upper bound (Ub)	Kp = 30, Ki = 10
Lower bound (Lb)	Kp = 10, Ki = 0
Objective function	ITAE

$$Xnew = \frac{X1+X2+X3}{3} \quad (31)$$

After finding the *Xnew*, the fitness value can be calculated. Then, the greedy solution is founded by comparing the current and old value and taking the best value. Several parameters and GWO values used to calculate PI for FOC in this study are shown in Table 3.

III. Results and Discussions

Overall, the system of this research is shown in Figure 6. FOC for induction motor using FYA and GWO algorithm PI tuning. The results of this research consist of two results. The first result shows the traction motor results for Jabodebek LRT at no-load conditions. The second condition is when the train passes a maximum height of 29 ‰ which can be illustrated in Figure 7. The second result is a comparison of the current response, electromagnetic torque, and speed with PI hand-tuning, FYA tuning, and GWO-tuning.

The initial simulation was conducted under no-load conditions. Through manual tuning, the proportional gain (Kp) and integral gain (Ki) for the speed controller were set to 20 and 1, respectively. Using the Firefly algorithm (FYA), the optimal values obtained were Kp = 10.985941 and Ki = 1.420272. Figure 8 presents

Figure 7. Train simulation conditions that include a 29 ‰ road slope.

the inverter output voltage under FOC control, which remains stable at the rated value of 499.304 volts.

Although no load is initially applied, a significant current surge peaking at approximately 397.878 A occurs during the startup of the train's traction motor A subsequent simulation involving a 29‰ gradient reveals a notable current increase from 35.8 A at 2.9 seconds to 172.863 A at 3 seconds, followed by a decrease to 37.6 A at 4.6 seconds.

Figure 9 illustrate the inverter current profiles under no-load and loaded conditions, respectively. Meanwhile, the Grey Wolf optimizer (GWO) yielded Kp = 16.233861 and Ki = 0.526774. The speed responses resulting from the field-oriented control (FOC) method using manual tuning, FYA, and GWO are illustrated in Figure 10. A clear distinction is observed between these two cases, particularly when the motor operates under load or climbs the incline, where elevated current levels are evident not only at startup but also during continued operation.

The Field-Oriented Control (FOC) system's performance is evaluated under zero load using three PI tuning methods, such as manual tuning, Firefly Algorithm (FYA), and Grey Wolf Optimizer (GWO), based on their motor speed responses. The hand-tuned

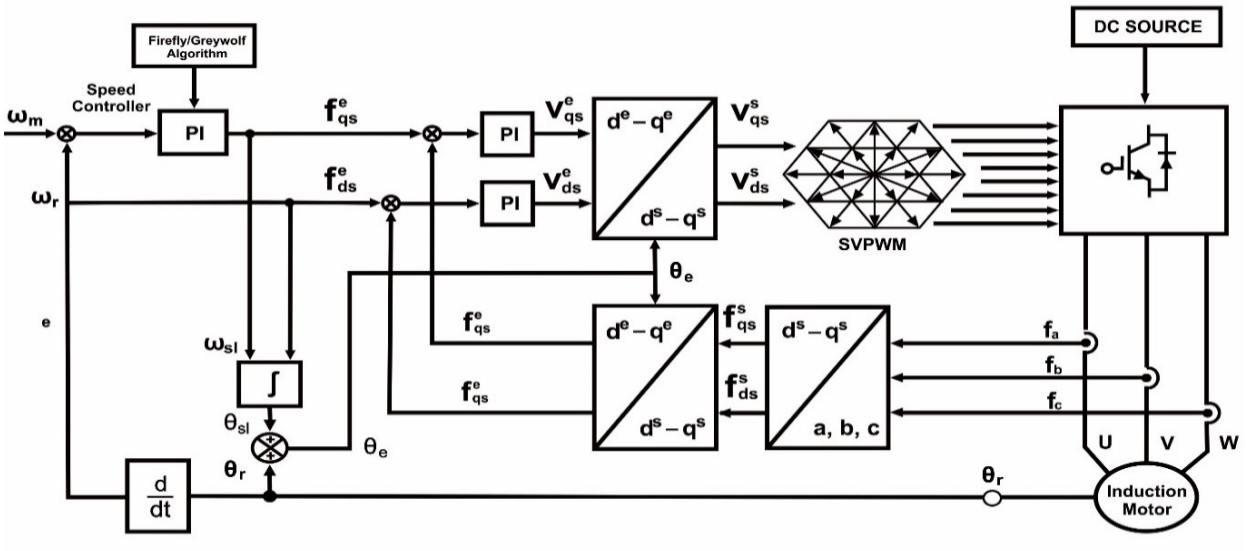

Figure 6. FOC for induction motor using FYA and GWO PI tuning.

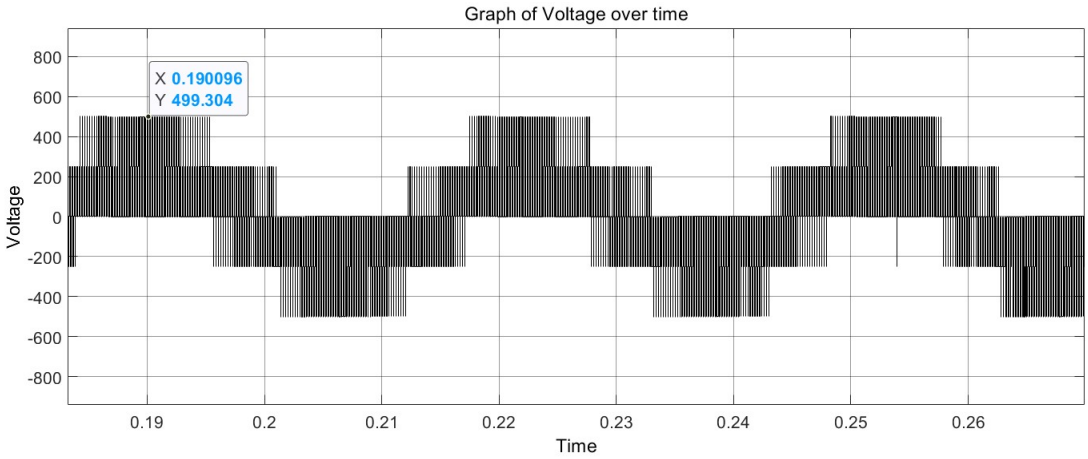

Figure 8. Inverter voltage using FOC for induction motor.

PI parameters is illustrated in Figure 10 (a). The motor reaches the steady-state speed of approximately 1521.83 rpm at around 0.79216 seconds. The response is relatively fast, but it shows a slight overshoot above the reference speed of 1500 rpm, indicating a potential trade-off between speed and precision in manual tuning.

Figure 10 (b) illustrates the speed response with PI parameters tuned using the Firefly Algorithm. The system reaches a steady-state speed of 1525.52 rpm around 1.14 seconds. Although the final speed is closer to the reference, the time required to settle is longer, and the overshoot is more pronounced than the hand-tuned method. This suggests that while FYA may optimize parameter search, it may not always achieve optimal dynamic performance without additional constraints. Figure 10.c shows the speed response using the Grey Wolf optimizer (GWO) for PI tuning. The system achieves steady-state at approximately 1520.72 rpm around 0.99 seconds, showing a good balance between fast response and minimal overshoot.

Compared to both hand-tuning and FYA, the GWO-based PI tuning offers a quicker response than FYA and a smoother convergence than hand-tuning. Overall, the GWO-based tuning yields the most favorable performance in terms of response speed, overshoot control, and steady-state accuracy, making it a superior method for tuning PI controllers in FOC applications under no-load conditions. This suggests that metaheuristic optimization methods such as GWO can effectively enhance system dynamics and reduce reliance on manual trial-and-error tuning, particularly for complex nonlinear systems like motor drives.

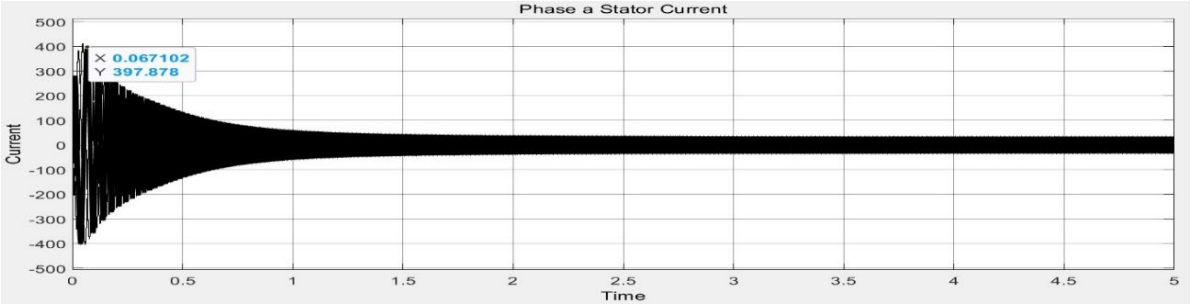

(a)

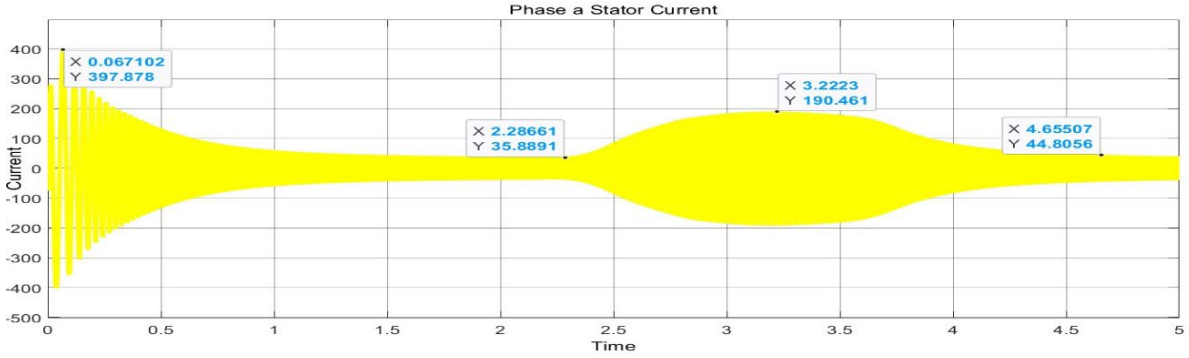

(b)

Figure 9. (a) Inverter current using FOC for induction motor in zero load; (b) Inverter current using FOC for induction motor with load.

The FOC system's performance under load is assessed by comparing motor speed responses using manual tuning, FYA, and GWO are illustrated in Figure 11. The 29 ‰ gradient introduces disturbances that highlight each method's robustness and adaptability. Figure 11 (a) depicts the response using hand-tuned PI parameters. The motor speed reaches a steady-state of approximately 1526.56 rpm at 0.82 seconds, slightly overshooting the 1500 rpm reference. The system shows significant sensitivity to the applied load disturbance, dropping to 1152.54 rpm at 3.22 seconds, before gradually recovering to 1527.26 rpm by 3.96 seconds. This oscillatory behavior indicates limited disturbance rejection and moderate recovery time, highlighting the limitations of manual tuning under dynamic load conditions with Kp = 20 and Ki = 1.

Firefly algorithm (FYA) for PI tuning motor speed response is illustrated in Figure 11 (b) The system

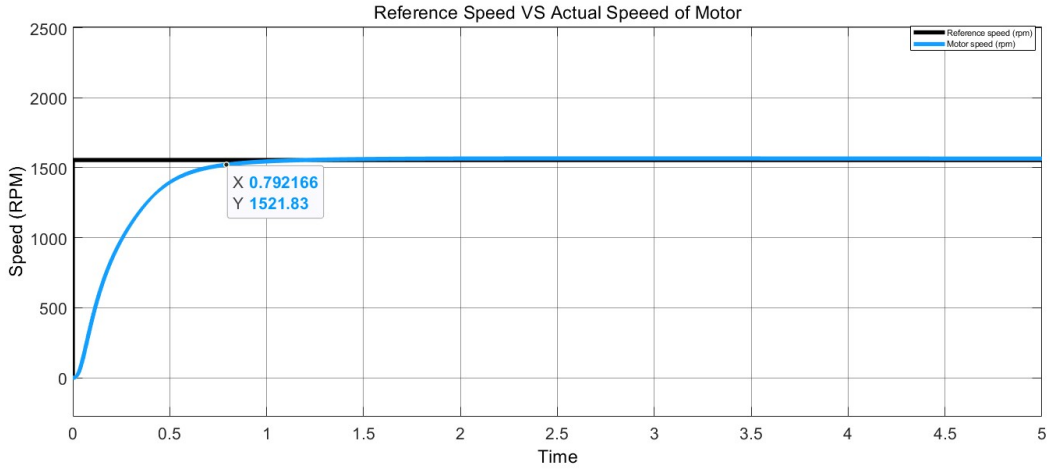

(a)

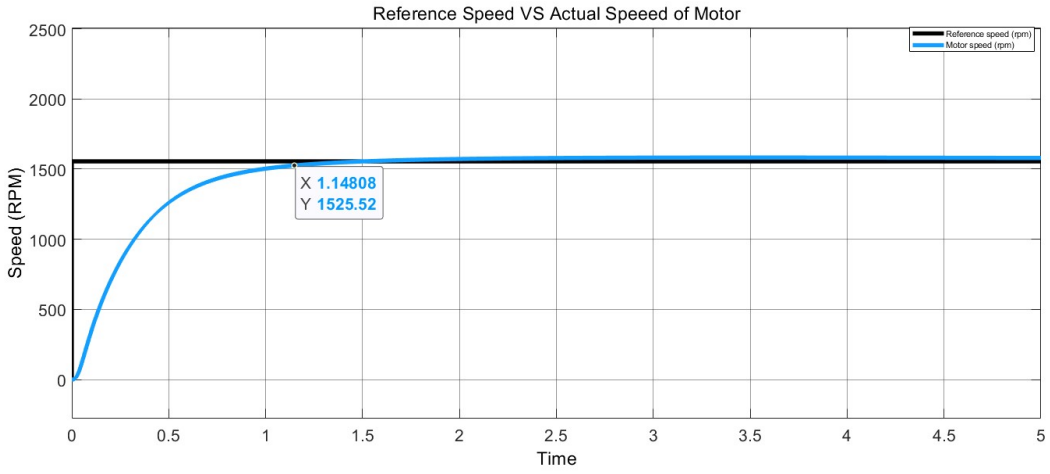

(b)

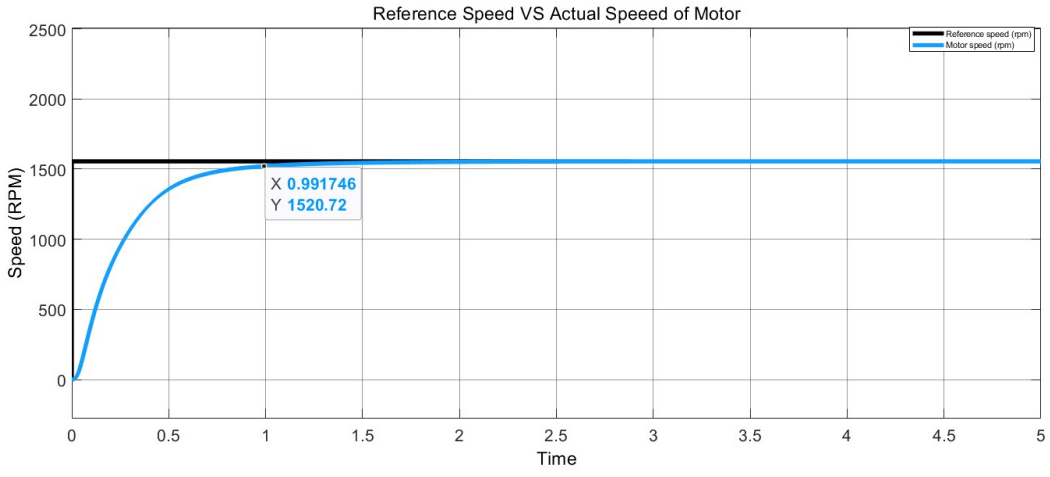

(c)

Figure 10. (a) a Speed response FOC of hand-tuning PI with zero load; (b) Speed response FOC of FYA PI tuning with zero load; (c) Speed response FOC of GWO PI tuning with zero load.

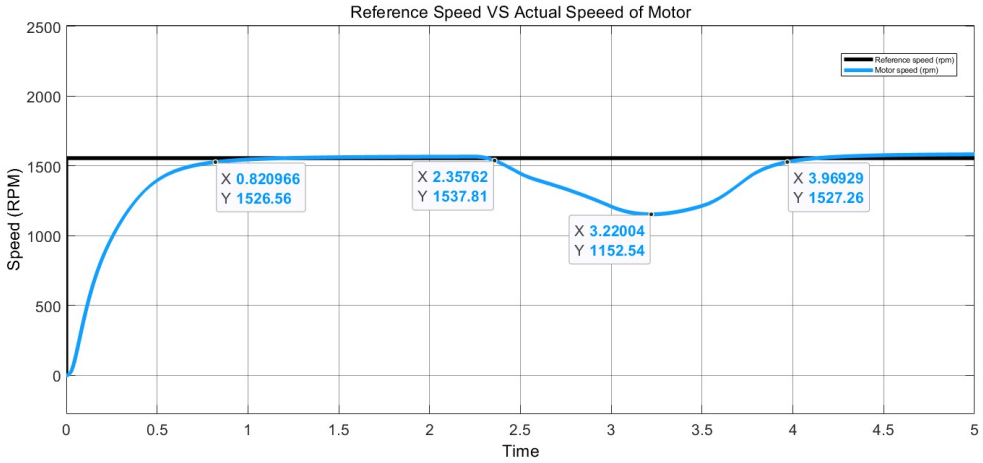

(a)

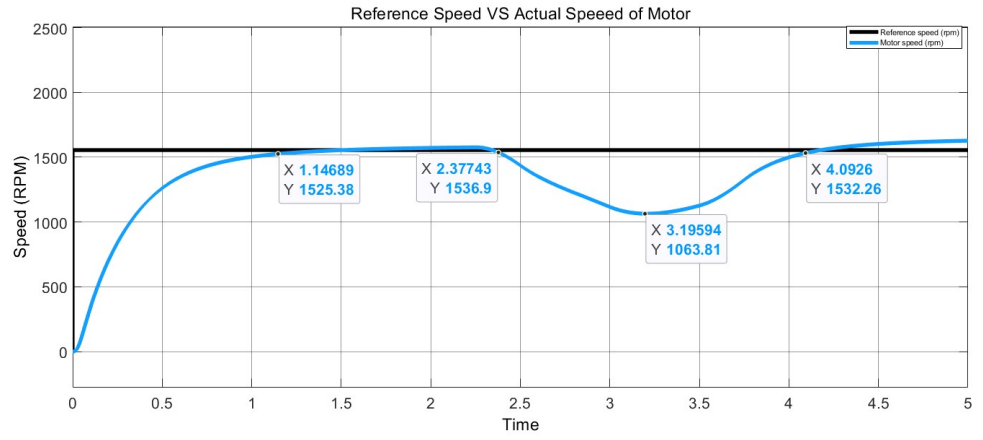

(b)

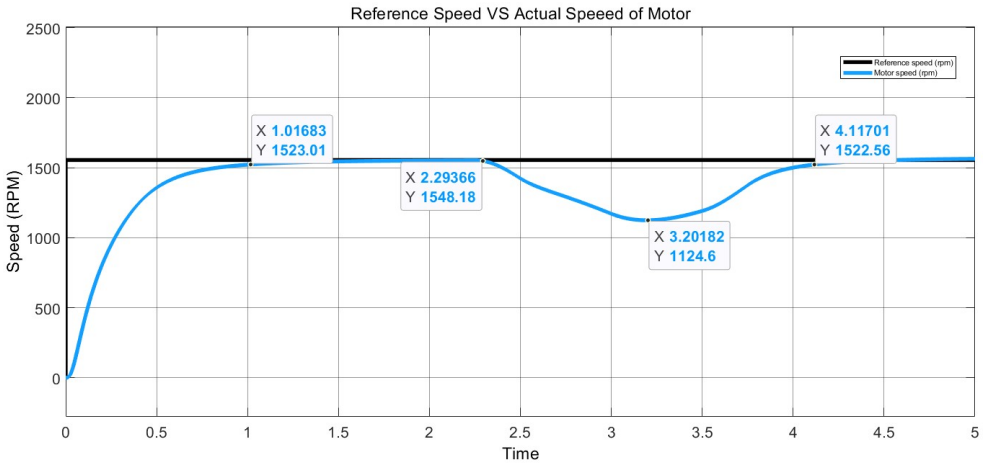

(c)

Figure 11. (a) Speed response FOC of hand-tuning with load; (b) Speed response FOC of FYA PI tuning with load; (c) Speed response FOC of GWO PI tuning with load.

achieves 1525.38 rpm at 1.14 seconds, overshooting to 1536.9 rpm, and then dipping to a minimum of 1063.81 rpm at 3.19 seconds due to the load disturbance. Recovery to 1532.26 rpm is observed by 4.09 seconds. Compared to hand-tuning, the FYA method shows more severe speed deviation and slower disturbance compensation, suggesting that its tuning outcome may lack robustness under load variation, despite achieving good performance in no-load scenarios. The Kp and Ki values were calculated with the difference in ITAE using FYA, so that it can be found that the Kp value is 10.985941 and Ki is 1.420272.

Figure 11 (c) demonstrates the response using the Grey Wolf Optimizer (GWO) for PI tuning. The motor reaches 1523.01 rpm at 1.01 seconds and exhibits a smoother transition with a peak at 1548.18 rpm and a disturbance-induced drop to 1124.6 rpm at 3.20 seconds. The system then recovers to 1522.56 rpm by 4.11 seconds. This method uses Kp 16.233861 and Ki 0.526774. Among the three methods, the GWO

approach shows a better balance between fast convergence, minimal overshoot, and quicker recovery from disturbances.

The GWO-based controller effectively reduces undershoot and stabilizes faster than both hand-tuning and FYA. Although all methods experience a notable speed drop due to the applied load, their recovery and overshoot responses differ. GWO consistently delivers better transient and steady-state performance, indicating greater robustness against load-induced disturbances. These results highlight the advantage of metaheuristic approaches, particularly GWO, in developing resilient control systems for induction motor drives under varying load conditions. All simulation results related to speed are summarized and illustrated in Table 4.

Figure 12 illustrated electromagnetic torque respond. Figure 12 (a) displays the torque response from the hand-tuned PI controller. At the initial moment, a significant torque spike reaching 275.315

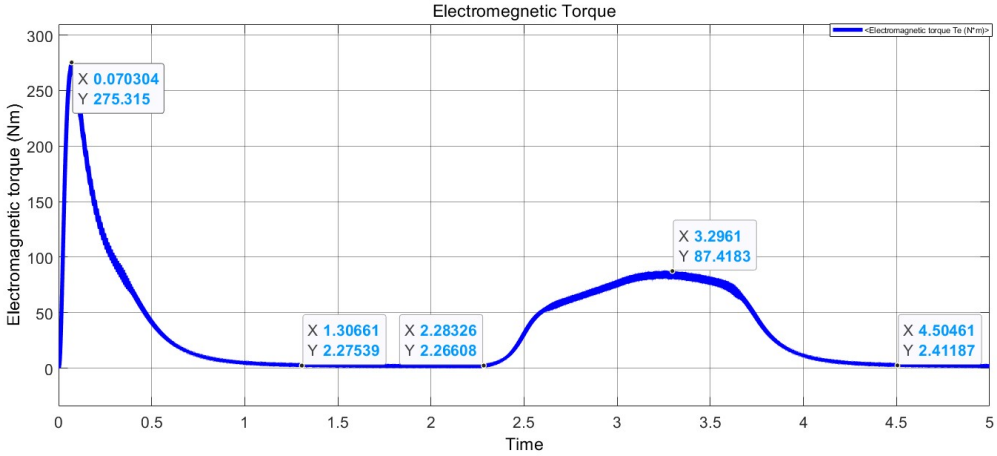

(a)

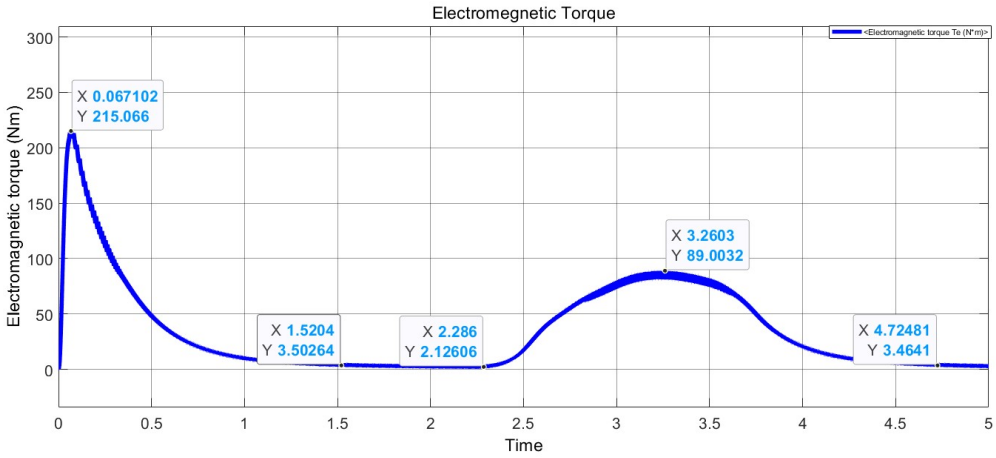

(b)

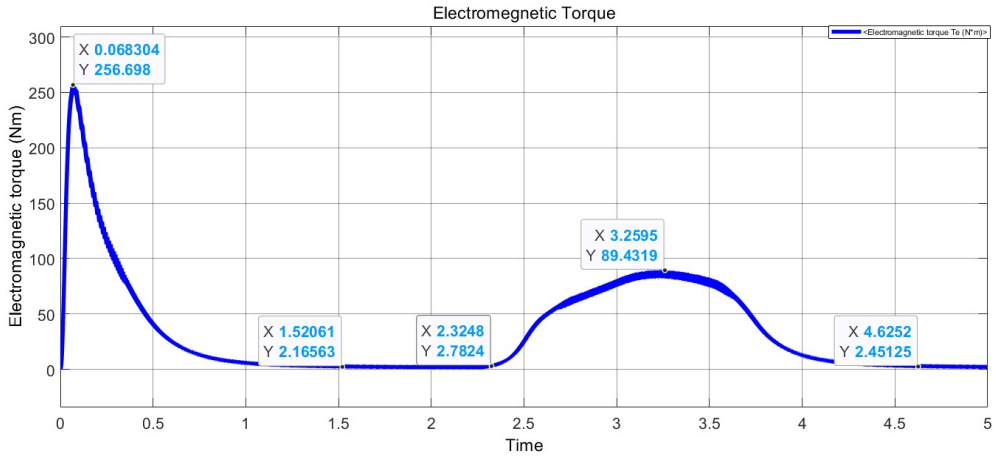

(c)

Figure 12. (a) Electromagnetic torque respond from FOC hand-tuning PI tuning with load; (b) Electromagnetic torque respond from FOC FYA PI tuning with load; (c) Electromagnetic torque respond from FOC GWO PI tuning with load.

Table 4.
The result of PI-tuning in all methods for speed.

Types	Kp	Ki	Rise point time	Start fall point		Maximum speed fall point		Speed rise back point		Condition
				Time	Speed	Time	Speed	Time	Speed	
Hand-tuning	20	1	0.79216	-	-	-	-	-	-	No load
			0.82096	2.3576	1537.81	3.22004	1152.54	3.96929	1527.26	Load (end-stable)
FYA	10.985941	1.420272	1.14808	-	-	-	-	-	-	No load
			1.14689	2.3774	1536.9	3.19594	1063.81	4.0926	1532.26	Load (end-unstable)
GWO	16.233861	0.526774	0.99174	-	-	-	-	-	-	No load
			1.01683	2.2936	1548.18	3.20182	1124.6	4.11701	1522.56	Load (end-stable)

Table 5.
The result of PI-tuning in all methods of electromagnetic torque.

Types	Kp	Ki	Start rising point		Maximum surge when loaded		Condition
			Time	Torque	Time	Torque	
Hand-tuning	20	1	0.0703	275.315	3.2961	87.4183	Load
FYA	10.985941	1.420272	0.0671	215.066	3.2603	89.0032	Load
GWO	16.233861	0.526774	0.0683	256.698	3.2595	89.4319	Load

Nm occurs at 0.07 seconds, which reflects a high transient torque during motor startup. The torque quickly settles to approximately 2.27 Nm, indicating steady-state operation. However, a second rise occurs at 3.22 seconds, peaking at 87.42 Nm, which corresponds to the motor compensating for an external load disturbance. Although it returns to near steady-state by 4.50 seconds, this profile suggests less stable disturbance rejection and relatively larger torque oscillations.

Figure 12 (b) presents the response from the FYA-based PI controller. The initial peak is lower than hand-tuning at 215.066 Nm, occurring at 0.067 seconds, implying a more conservative torque injection during startup. The steady-state torque remains low around 2.12–3.5 Nm, but the system experiences a large disturbance torque of 89.0032 Nm at 3.26 seconds, similar in magnitude to the hand-tuned case. The slower and wider torque ripple indicates delayed compensation to load changes, reflecting reduced dynamic responsiveness and stability.

The GWO-based PI tuning results are illustrated in Figure 12 (c). The startup torque spike reaches 256.698 Nm at 0.068 seconds, close to the hand-tuning case. The torque quickly drops and stabilizes from 2.16 to 2.78 Nm, indicating efficient transition into steady-state. A disturbance-induced rise occurs at 3.26 seconds, peaking at 89.4319 Nm, followed by a smoother recovery and stabilization at 2.45 Nm by 4.62 seconds. The GWO response shows a controlled and well-damped torque profile, effectively balancing dynamic torque demand and system stability. To support the interpretation of the torque simulation results, Table 5 presents the experimental torque data obtained using various methods.

In summary, all three tuning methods show strong initial torque transients due to acceleration, followed by a response to load disturbance. However, the GWO method provides the most balanced performance: lower steady-state ripple, faster stabilization afterdisturbance, and adequate torque generation to overcome load changes without excessive oscillation. This demonstrates GWO's superior ability to optimize PI parameters not only for speed control but also for effective torque regulation, which is crucial in applications requiring both precision and stability under varying load conditions.

IV. Conclusion

The Grey Wolf optimizer (GWO) method demonstrated the most effective performance among the three PI tuning strategies for the Jabodebek LRT traction motor. GWO provided a well-balanced dynamic response, with faster torque rise, minimal speed fluctuation under load, and superior recovery characteristics. The Firefly algorithm (FYA) also showed adequate regulation but was less robust during dynamic disturbances. In contrast, the hand-tuning method, with fixed gain values, resulted in slower response and less optimal performance under varying load conditions. Overall, optimization-based approaches, particularly GWO, significantly enhance control accuracy and system stability in traction applications. For future studies, it is recommended to explore hybrid optimization methods or adaptive

control strategies that can dynamically adjust PI parameters in real time based on operating conditions. Additionally, the integration of machine learning techniques to predict and mitigate disturbance effects could further improve performance and robustness in complex rail traction systems.

Declarations

Author contribution

Wahyu Pribadi: supervision, investigation, and funding acquisition. **Ricto Yudi Wicaksono**: simulation and AI tuning design, conceptualization, investigation, validation, and data curation. **Darma Arif Wicaksono, Rakhmad Gusta Putra**: original draft writing and review-editing. **Moh. Lutfi Yazid**: resource provision, investigation, and validation in the factory field.

Funding statement

The author extends sincere gratitude to the Madiun State Polytechnic for their generous provision of internal competitive research funding. Through this valuable support and collaborative synergy, we have been able to acquire significant and beneficial knowledge.

Competing interest

The authors declare that they have no known competing financial interests or personal relationships that could have appeared to influence the work reported in this paper.

Additional information

Reprints and permission: information is available at https://mev.brin.go.id/.

Publisher's Note: National Research and Innovation Agency (BRIN) remains neutral with regard to jurisdictional claims in published maps and institutional affiliations.

References

[1] M. Thoriq Maulana, M. Hilmi Habibullah, Sunandar, N. Sholihah, M. Ainul Rifqi L. P., and F. Fahrudin, "Kegiatan pemantauan kualitas udara provinsi DKI Jakarta tahun 2022," *Lap. Akhir*, vol. 1, no. 201310200311137, pp. 78–79, 2015, [Online].

[2] B. P. Statistik, "Berita resmi statistik No.11/03/31/Th.XXVI, 1 Maret 2024," vol. 2023, no. 11, pp. 1–8, 2024, [Online].

[3] D. Pribula, A. Dolinayova, and M. Kendra, "Alternative Propulsion in Railway Passenger Transport - The Way to Green Transport," *Transp. Res. Procedia*, vol. 77, no. 2023, pp. 43–50, 2024.

[4] I. Riabov, S. Goolak, L. Kondratieva, and L. Overianova, "Increasing the energy efficiency of the multi-motor traction electric drive of an electric locomotive for railway quarry transport," *Eng. Sci. Technol. an Int. J.*, vol. 42, p. 101416, 2023.

[5] M. Z. Romdlony and F. Irsyadi, "Hardware-in-the-loop simulation of DC motor as an instructional media for control system design and testing," *J. Mechatronics, Electr. Power, Veh. Technol.*, vol. 12, no. 2, pp. 81–86, 2021.

[6] S. Nategh *et al.*, "A review on different aspects of traction motor design for railway applications," *IEEE Trans. Ind. Appl.*, vol. 56, no. 3, pp. 2148–2157, 2020.

[7] Sang-Hoon Kim, "*Electric motor control: DC, AC, and BLDC motors*," Amsterdam, Netherlands: Elsevier, 2017. [Online].

[8] B. D. Hughes Austin, *Electric Motors and Drives*, 5th ed., vol. 11, no. 1. The Boulevard, Langford Lane, Kidlington, Oxford OX5 1GB, United Kingdom 50 Hampshire Street, 5th Floor, Cambridge, MA 02139, United States: Elsevier Ltd., 2019.

[9] Menteri Perhubungan Republik Indonesia, "Peraturan Menteri Perhubungan Nomor 60 Tahun 2012 tentang Persyaratan Teknis Jalur Kereta Api," *Kementrian Perhub. Republik Indones.*, pp. 1–57, 2012, [Online].

[10] PT INKA, "Train Performance," MADIUN, 2020. [Online].

[11] C. Upendra Reddy, K. K. Prabhakar, A. K. Singh, and P. Kumar, "Speed estimation technique using modified stator current error-based MRAS for direct torque controlled induction motor drives," *IEEE J. Emerg. Sel. Top. Power Electron.*, vol. 8, no. 2, pp. 1223–1235, 2020.

[12] B. R. Vinod and G. Shiny, "Direct torque control scheme for a four-level-inverter fed open-end-winding induction motor," *IEEE Trans. Energy Convers.*, vol. 34, no. 4, pp. 2209–2217, 2019.

[13] X. Wu, W. Huang, X. Lin, W. Jiang, Y. Zhao, and S. Zhu, "Direct torque control for induction motors based on minimum voltage vector error," *IEEE Trans. Ind. Electron.*, vol. 68, no. 5, pp. 3794–3804, 2021.

[14] R. K. Bindal and I. Kaur, "Torque ripple reduction of Induction Motor using Dynamic Fuzzy Prediction Direct Torque Control," *ISA Trans.*, vol. 99, pp. 322–338, 2020.

[15] Y. Qu, B. Zhang, H. Chu, H. Shen, J. Zhang, and X. Yang, "Sliding-mode anti-disturbance speed control of permanent magnet synchronous motor based on an advanced reaching law," *ISA Trans.*, vol. 139, pp. 436–447, 2023.

[16] D. Zellouma, Y. Bekakra, and H. Benbouhenni, "Field-oriented control based on parallel proportional–integral controllers of induction motor drive," *Energy Reports*, vol. 9, pp. 4846–4860, 2023.

[17] H.-G. H. Mirza Abdul Waris Begh, "Comparison of field oriented controland direct torque control," *TechRxiv*, pp. 1–16, 2018.

[18] A. P. Widyadharma *et al.*, "Close loop speed control design for 3ø induction motor on electric railway with

embedded PID controller," *Int. Res. J. Adv. Eng. Sci.*, vol. 7, no. 3, pp. 210–213, 2022. [Online].

[19] S. Chandrasekaran, S. Durairaj, and S. Padmavathi, "A performance evaluation of a fuzzy logic controller-based photovoltaic-fed multi-level inverter for a three-phase induction motor," *J. Franklin Inst.*, vol. 358, no. 15, pp. 7394–7412, 2021.

[20] Z. M. S. Elbarbary, O. K. Al-Harbi, S. F. Al-Gahtani, S. M. Irshad, A. Y. Abdelaziz, and M. A. Mossa, "Review of speed estimation algorithms for three- phase induction motor," *MethodsX*, vol. 12, no. August 2023, p. 102546, 2024.

[21] I. Anshory *et al.*, "Optimization DC-DC boost converter of BLDC motor drive by solar panel using PID and firefly algorithm," *Results Eng.*, vol. 21, no. December 2023, p. 101727, 2024.

[22] E. saadi Terfia, S. Mendaci, S. E. Rezgui, H. Gasmi, and W. Kantas, " Optimal third-order sliding mode controller for dual star induction motor based on grey wolf optimization algorithm," *Heliyon*, vol. 10, no. 12, p. e32669, 2024.

[23] I. I. Novendra, I. M. Wirawan, A. Kusumawardana, and A. K. Latt," Optimization of load frequency control using grey wolf optimizer in micro hydro power plants," *J. Mechatronics, Electr. Power, Veh. Technol.*, vol. 14, no. 2, pp. 166–176, 2023.

[24] H. A. Toliyat and S. G. Campbell, "*DSP-based electromechanical motion control*," Boca Raton, Fl: CRC Press, 2004. [Online].

[25] P. C. Krause, O. Wasynczuk, S. D. Sudhoff, and S. D. Pekarek, "Analysis of Electric Machinery and Drive Systems," 4th ed. Hoboken, NJ: Wiley-IEEE Press (John Wiley & Sons), 2025.

[26] A. Almabrok, M. Psarakis, and A. Dounis, "Fast tuning of the PID controller in an HVAC system using the Big Bang-Big Crunch algorithm and FPGA technology," *Algorithms*, vol. 11, no. 10, 2018.

[27] W. A. Khan, N. N. Hamadneh, S. L. Tilahun, and J. M. T. Ngnotchouye, "A review and comparative study of firefly algorithm and its modified versions," *Optim. Algorithms - Methods Appl.*, 2016.

[28] M. S. Shaikh, C. Hua, M. A. Jatoi, M. M. Ansari, and A. A. Qader, "Application of grey wolf optimisation algorithm in parameter calculation of overhead transmission line system," *IET Sci. Meas. Technol.*, vol. 15, no. 2, pp. 218–231, 2021.

[29] D. Awasthi, A. Tiwari, P. Khare, and V. K. Srivastava, "A comprehensive review on optimization-based image watermarking techniques for copyright protection," *Expert Syst. Appl.*, vol. 242, no. 122830, 2024.